SAND2016-2400C

Sensing delamination in epoxy encapsulant systems with fiber Bragg gratings

Brad H. Jones*[a], Garth D. Rohr[a], Amy K. Kaczmarowski[a]
[a]Sandia National Laboratories, P.O. Box 5800, Albuquerque, NM 87185

ABSTRACT

Fiber Bragg gratings (FBGs) are well-suited for embedded sensing of interfacial phenomena in materials systems, due to the sensitivity of their spectral response to locally non-uniform strain fields. Over the last 15 years, FBGs have been successfully employed to sense delamination at interfaces, with a clear emphasis on planar events induced by transverse cracks in fiber-reinforced plastic laminates. We have built upon this work by utilizing FBGs to detect circular delamination events at the interface between epoxy films and alumina substrates. Two different delamination processes are examined, based on stress relief induced by indentation of the epoxy film or by cooling to low temperature. We have characterized the spectral response pre- and post-delamination for both simple and chirped FBGs as a function of delamination size. We show that delamination is readily detected by the evolution of a non-uniform strain distribution along the fiber axis that persists after the stressing condition is removed. These residual strain distributions differ substantially between the delamination processes, with indentation and cooling producing predominantly tensile and compressive strain, respectively, that are well-captured by Gaussian profiles. More importantly, we observe a strong correlation between spectrally-derived measurements, such as spectral widths, and delamination size. Our results further highlight the unique capabilities of FBGs as diagnostic tools for sensing delamination in materials systems.

Keywords: fiber Bragg grating, delamination, interface, epoxy, ceramic, embedded sensing, strain distribution, chirped

1. INTRODUCTION

Thermosetting polymers are derived from the conversion of a liquid mixture of one or more multifunctional compounds into an infusible solid. Epoxies are a particularly important class of thermosets, typically consisting of a diepoxide cured by a multifunctional alcohol or amine. Due to their toughness and chemical inertness, as well as their relatively low cost, epoxies are used as encapsulants to isolate, insulate, and protect a variety of sensitive devices from adverse chemical, mechanical, and thermal conditions. By its very nature, however, encapsulation involves the creation of interface between dissimilar materials, invariably leading to the development of internal residual stresses in the encapsulant during processing and use. For example, epoxies undergo significant volumetric shrinkage during cure, yet adhesion to an encapsulated component prevents this shrinkage from occurring isotropically. Furthermore, the mismatch in thermal expansion between an epoxy and an encapsulated component imposes similar constraints during temperature excursions. If the magnitude of the resulting stresses is large enough, adhesive failure (*i.e.*, delamination) may occur as a stress relief mechanism, with concomitant failure or reduced performance of the encapsulated device.

In many encapsulated systems, particularly those utilizing filled encapsulants, there may be no outward indicators of delamination. Therefore, a clear need exists for passive techniques by which the occurrence of delamination can be detected, free of any deleterious effects to encapsulant and overall device performance. To this end, fiber optic-based technologies have been developed for a variety of chemical, mechanical, and thermal sensing applications, driven in part by the ease of embedment of fibers and their minimally invasive nature. More specifically, fiber Bragg gratings (FBGs) have been extensively studied as embedded strain sensors capable of highly sensitive measurements of local, non-uniform strain distributions.[1-11] The distinguishing feature of FBGs is a periodic variation in refractive index that is written into the fiber core by UV light using a phase mask[12] or interference lithography.[13] This periodic variation, or grating, reflects light that satisfies the Bragg condition, with a wavelength proportional to refractive index and grating period. A mechanical deformation imposed on the grating will alter these properties; hence, time-resolved measurement of reflected wavelength provides a means of monitoring such deformation. Numerous publications have described and validated methodologies for evaluating FBG axial strain from reflected wavelength shifts.[14-16] Even further, chirped gratings with non-uniform grating periods have been exploited to evaluate non-uniform axial strain profiles, as chirped FBGs exhibit broadband reflectance where the distribution in reflected wavelength can be mapped to grating coordinates.[1-11] Although the quantitative evaluation of non-uniform strain distributions from spectral perturbations is far

from straightforward, several groups have employed recursive methods to calculate complex profiles with remarkable accuracy.[3,5,9,11]

To date, FBGs have been embedded in a variety of materials systems and used to study failure processes, including delamination.[17-33] Much of the work concerning delamination has focused on fiber-reinforced polymers. For example, Takeda, Okabe, *et al*. embedded uniform and chirped FBGs at ply interfaces in laminated, carbon fiber-reinforced, polymer panels and subjected the panels to bending loads to propagate interfacial delaminations.[19,22] They showed correlations between key characteristics of the FBG reflected spectra and crack length. In addition, they used finite element modeling (FEM) to predict strain distributions along the gratings, calculated the corresponding reflected spectra, and found good qualitative agreement with the measured spectra. More recently, Sanderson, *et al*. studied delamination growth at the interface between nylon and a glass fiber-reinforced epoxy using a chirped FBG mounted on the surface of a double-cantilevered beam.[31] Similar to the previous example, they demonstrated that the crack length in this geometry could be accurately calculated from the positions of local minima in the FBG reflected spectrum, corresponding to non-uniform compressive strain distributions.

In this paper, we report our preliminary investigation of delamination at polymer-ceramic interfaces using embedded FBGs. Ceramics and polymers generally possess disparate surface chemistries that may cause poor adhesion when encapsulating ceramic components. Moreover, ceramics and polymers are characterized by comparatively low and high thermal expansion coefficients, respectively, leading to large thermal stresses in encapsulated systems. Due to these collective phenomena, polymer-ceramic interfaces are particularly susceptible to delamination. We have embedded simple and chirped FBGs in epoxy films cured on alumina substrates and studied the FBG reflected spectra in response to mechanically- and thermally-induced delamination (Figure 1). In the former case, the epoxy film is indented at constant temperature, causing a circular crack to propagate outward from the indenter tip along the epoxy-alumina interface with increasing load. In the latter case, a region of poor adhesion at the epoxy-alumina interface is created through a simple surface treatment, and subsequent temperature cycling results in preferential delamination within this region.

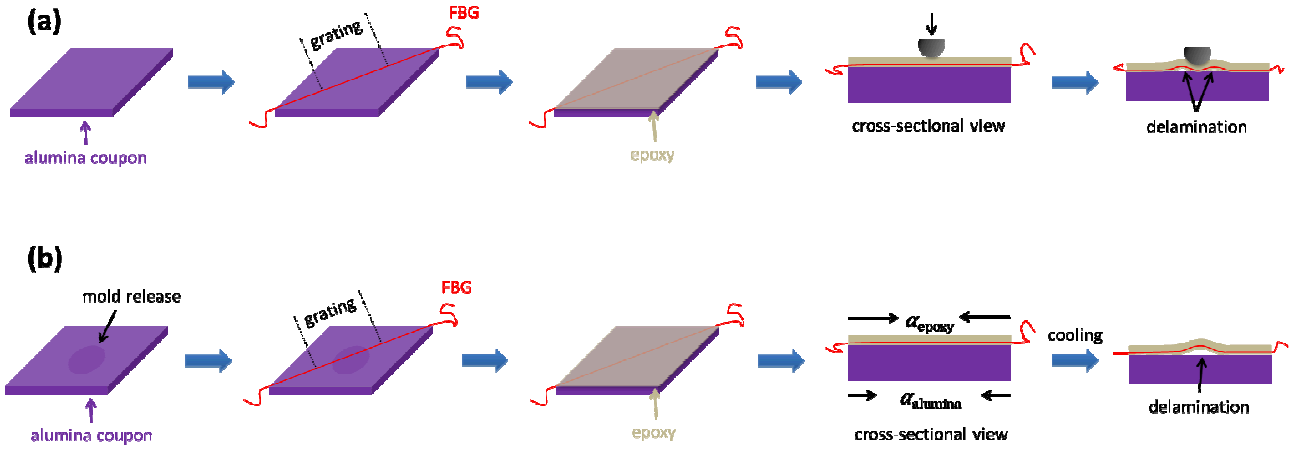

Figure 1. Schematic diagram of processes for **(a)** mechanically-induced and **(b)** thermally-induced delamination at epoxy-alumina interfaces. In **(a)**, a FBG is laid on an alumina coupon and epoxy is potted around the FBG. The resulting epoxy film is indented, during which mechanical stress is relieved by delamination at the interface. In **(b)**, a portion of an alumina coupon is coated with mold release. A FBG is laid on the coupon and epoxy is potted around the FBG. During subsequent cooling, the thermal stress from mismatch in the coefficients of thermal expansion (α) is relieved by delamination at the interface.

2. METHODOLOGY

2.1 Materials

EPON™ 828 – an oligomeric diglycidyl ether of bisphenol A – was obtained from Momentive (Waterford, NY, USA). Diethanolamine (DEA) was obtained from Acros Organics (Geel, Belgium). Ultra II Epoxy Parfilm mold release was

obtained from Price Driscoll (Waterford, CT, USA), supplied as a paintable, liquid solution. An alumina-based ceramic of proprietary composition was obtained from CerCo (Shreve, OH, USA). This ceramic was processed into square coupons of dimensions 1 in x 1 in x 0.096 in and the coupons were ultrasonically cleaned prior to use.

Simple FBGs were obtained from Micron Optics (Atlanta, GA, USA), sold under the model name os1100. Chirped FBGs were obtained from O/E Land (Lasalle, Canada), sold under the model name OEFBG-100. All FBGs are polyimide-coated with diameter ~ 150 μm and grating length 10 mm.

2.2 Indentation Tests

A schematic diagram of the process used for indentation testing is shown in Figure 1(a). A single FBG is laid on top of an alumina coupon and secured in place with Kapton® tape. EPON 828 and DEA are pre-heated to 71 °C and then mixed by hand in a 100:12 wt:wt ratio. A small drop of the mixed epoxy (~ 0.25 mL) is placed on a Teflon™ substrate and the coupon is placed FBG-side down to sandwich the epoxy between the coupon and substrate. The thickness of the epoxy film is controlled by placing several Teflon™ spacers around the edges of the coupon. The entire sandwich fixture is heated to 71 °C for 16 hr to cure the epoxy. After cooling to room temperature, the alumina coupon and adhered epoxy film with embedded FBG are removed from the substrate.

The epoxy-alumina coupon is placed in an environmental chamber and cooled to -55 °C. After reaching thermal equilibrium, the surface of the epoxy film is indented using a stainless steel spherical indenter of 0.0625 in diameter attached to an Instron 5565 Universal Testing Machine. The indentation rate was 0.05 mm/min, and FBG spectra were recorded before, during, and after the application of various loads ranging from 10-100 kg.

2.3 Thermal Tests

A schematic diagram of the process used for thermal testing is shown in Figure 1(b). Epoxy-alumina coupons are prepared in the same manner as described for indentation testing, with one key exception. In this case, the starting alumina coupon is first modified by depositing a film of mold release in the center of the coupon. A drop of Ultra II is placed on the coupon surface and allowed to dry, after which the FBG is laid on the coupon and epoxy is potted around the FBG as described above.

The epoxy-alumina coupon is then cooled to various temperatures. Mild cooling over the range of -100 °C to room temperature is accomplished by means of a liquid nitrogen-cooled environmental chamber. Severe cooling is accomplished by immersing the coupon directly in liquid nitrogen. FBG spectra were recorded before, during, and after thermal cycling.

2.4 FBG Analysis

The embedded FBGs were interrogated using a si255 optical sensing instrument from Micron Optics. This instrument features a swept-wavelength laser with a wavelength range of 1460-1620 nm, a 25 dB dynamic range, and a 1000 Hz maximum sampling frequency. FBG reflected spectra were recorded using Micron Optics ENLIGHT software package. The experimental spectra were compared to predicted spectra generated using OptiGrating software from Optiwave Systems (Nepean, Canada). This software approximates a grating as a series of uniform sub-gratings and applies a transfer matrix method to solve the coupled mode equations,[34] thereby enabling calculation of a grating's reflection.

3. RESULTS AND DISCUSSION

3.1 Mechanically-Induced Delamination

Figure 2 shows the results of a typical test in which epoxy films with embedded FBGs on alumina substrates are indented. The epoxy films in this particular example are approximately 500 μm thick. The penetration of the spherical indenter tip into the comparatively low-modulus epoxy (Young's modulus E ~ 3 GPa), coupled with its adhesion to the rigid alumina (E ~ 300 GPa) substrate, produces significant in-plane and out-of-plane stresses. At sufficiently high load, these stresses are partially relieved by the formation of a circular crack at the epoxy-alumina interface, *i.e.*, delamination. The circular crack front propagates with increasing load, while the delamination radius for a given applied load and film thickness reflects the adhesive strength of the interface.[35] In Figure 2(a) and Figure 2(c), the circular delamination is plainly apparent from the boundary between the light and dark purple regions. For this configuration, the 80 kg applied load produces a delamination radius of 1.62 mm ± 0.06 mm.

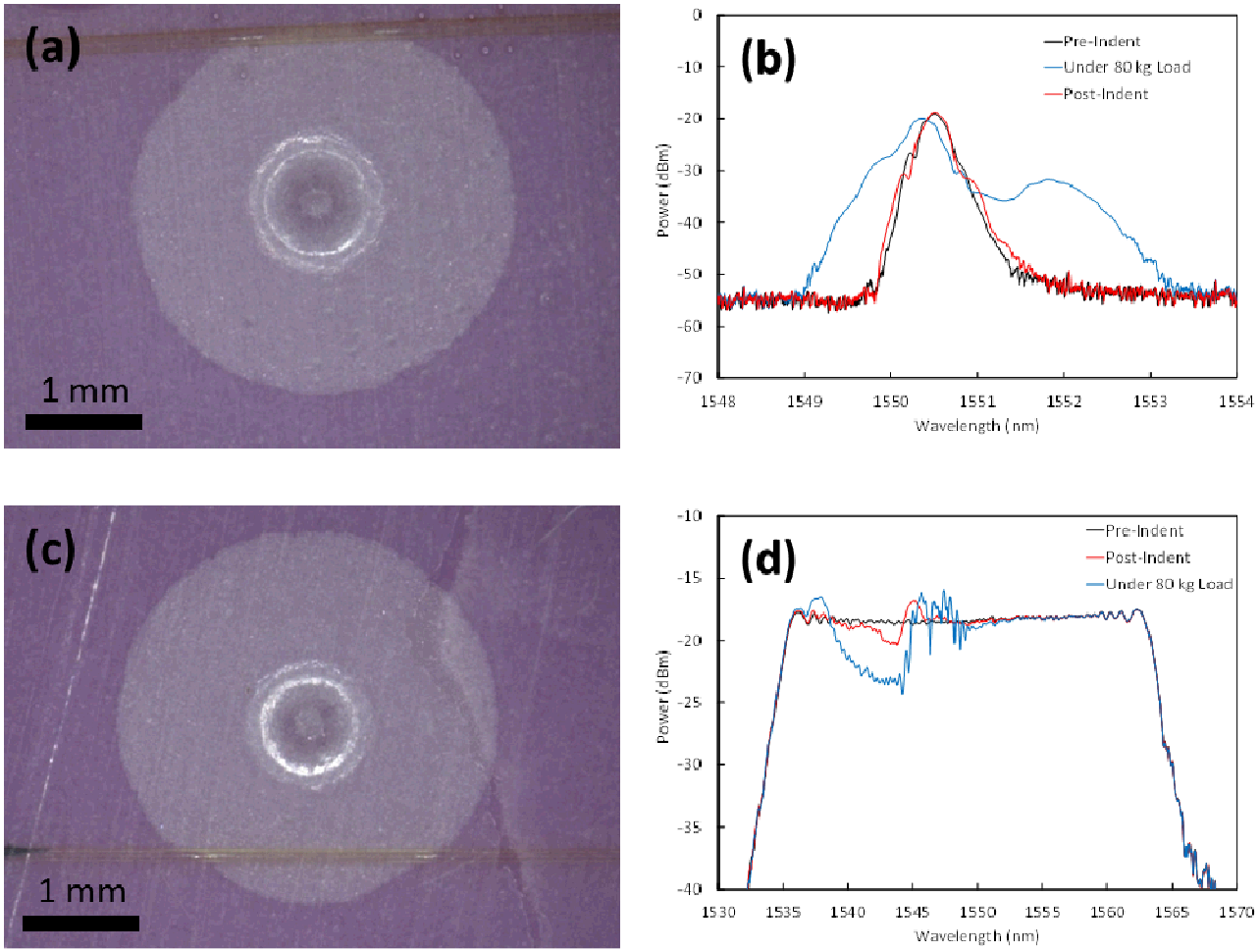

Figure 2. Plane-view optical micrographs of **(a)** simple FBG and **(c)** chirped FBG embedded in epoxy film on alumina coupon after 80 kg indentation, with corresponding reflected spectra – **(b)** simple, **(d)** chirped – before (black) and during (blue) application of load and after removal of load (red).

For the tests shown in Figure 2, we intentionally sought to position the indenter such that the FBG is located well off-center, but with a portion of the grating intersecting the area above the delamination. The area of epoxy film directly under the indenter tip experiences extremely large deformation magnitudes that fracture the fiber under these loading levels, as will be discussed in more detail later. Indeed, despite the off-center FBG orientation, the reflected spectra (Figure 2(b) and Figure 2(d)) indicate substantial localized strain in the fiber, particularly during application of load. Under load, both the simple and chirped FBG suggest a complex axial strain distribution along the grating, consisting of both compressive and tensile contributions. The narrow Bragg reflection of the simple FBG broadens substantially, exhibiting local maxima shifted +1.34 nm and −0.14 nm relative to the Bragg wavelength prior to indentation. These wavelength shifts correspond to an axial tensile microstrain of 1110 and an axial compressive microstrain of 119, respectively, using 0.22 as the photoelastic constant.[36] Similarly, the chirped FBG exhibits a region of reduced power in its broadband reflection, with increased power at higher and lower wavelengths indicating tensile and compressive strain, respectively. As with the simple FBG, the tensile contribution encompasses a broader wavelength range than the compressive contribution, reflecting that the strain distribution is predominantly tensile in nature.

After indentation and the removal of the indenter tip from the film, the FBG spectra (Figure 2(b) and Figure 2(d)) contain residual perturbations reflecting permanent deformation associated with delamination. The simple FBG shows very slight broadening of the Bragg reflection, whereas the chirped FBG shows a significant inflection point. It is important to note that the positions of the two FBGs relative to the indent center are not identical, thus precluding a quantitative comparison of strain; however, these data provide additional confirmation of the well-documented

sensitivity that a grating chirp provides for the detection of a non-uniform strain distribution. To further quantify the permanent strain experienced by the chirped FBG, we used OptiGrating software to examine the effect of various axial strain distributions on the grating reflection. As shown in Figure 3, a good match between the OptiGrating calculation and the measured spectrum is obtained by applying a Gaussian strain distribution to the former with a maximum microstrain of 600 and a full-width half-maximum of 0.83 mm. Interestingly, the distribution in Figure 3(b) spans approximately 2.1 mm of the grating length, which is identical to the length over which the grating intersects the delaminated area as measured from Figure 2(c). The Gaussian tensile strain used here also contrasts starkly with previous FBG measurements conducted near delaminations. For example, the reflected spectra from FBGs embedded near flexure-induced delaminations in composite panels have shown good agreement with calculated spectra derived using a step-function-like strain distribution.[19,22] Unsurprisingly, these differences suggest that the permanent strain associated with delamination is highly dependent on the deformation mode from which the delamination results.

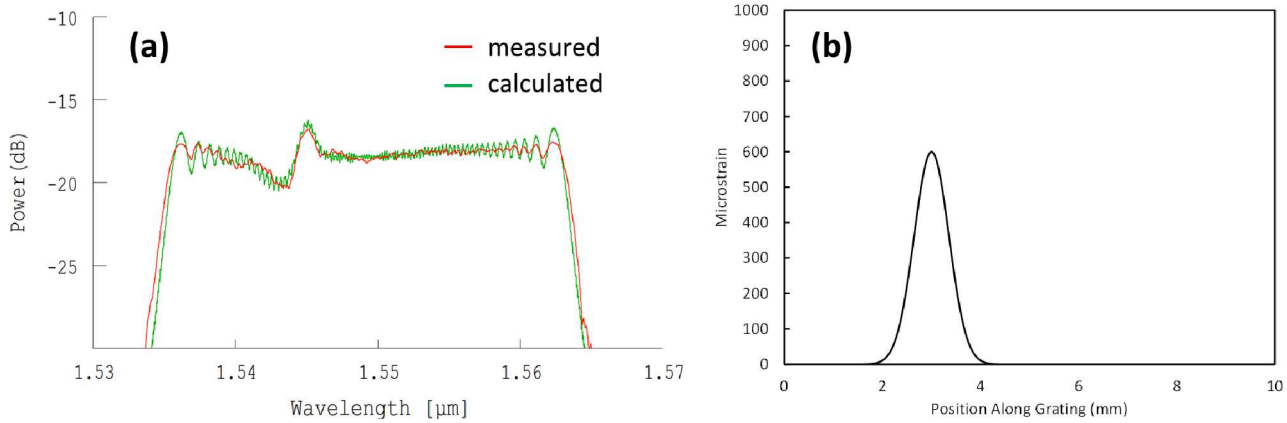

Figure 3. (a) Measured reflected spectrum (red) from a chirped FBG embedded in epoxy film on alumina coupon after 80 kg indentation compared to spectrum calculated using OptiGrating software (green). The experimental data correspond to the post-indent curve plotted in Figure 2(d). The grating parameters used in the calculation are core and cladding thicknesses 8 and 117 μm and refractive indices 1.449 and 1.444, respectively (based on SMF-28 fiber optic standard),[37] core refractive index modulation 1.15×10^{-4}, linear chirp 9.95 nm, and central wavelength 1549.3 nm. The axial strain profile used in the calculation is plotted in **(b)**, and 0.22 is used as the photoelastic constant.[36]

Inspired by our observation that the span in a permanent strain distribution derived from a FBG measurement coincided with delamination size, we examined correlations between spectral features and indentation conditions. In Figure 4(a), the post-indentation reflected spectra from an embedded, chirped FBG are plotted for varying loads and compared to the spectrum prior to indentation. The particular sample indented is identical to those described previously except, in this case, the indenter was oriented directly over the fiber. The spectra again reveal a permanent, non-uniform strain distribution in the film after indentation. At 65 kg applied load, the embedded fiber fractures and the reflected signal beyond the point of fracture is lost. Previous data have shown linear scaling between indentation load and delamination radius for epoxy films on glass substrates.[38] We chose to compare the indentation load in our experiment to the wavelength range, or spectral width, over which each post-indentation spectrum deviates from the pre-indentation spectrum (defined as the difference between the minimum and maximum wavelengths where the power difference exceeds a constant value). The choice of the latter quantity is motivated by the fact that the total broadband width is directly proportional to the grating length, while the deviated spectral width must scale with the span of the strain distribution. Therefore, we postulated that the spectral width may potentially scale with delamination size. This comparison is plotted in Figure 4(b), where a linear correlation between indentation load and the deviated spectral width is clearly observed. These data provide further validation that key spectral features from FBGs can be exploited to interrogate crack dimensions in materials systems.

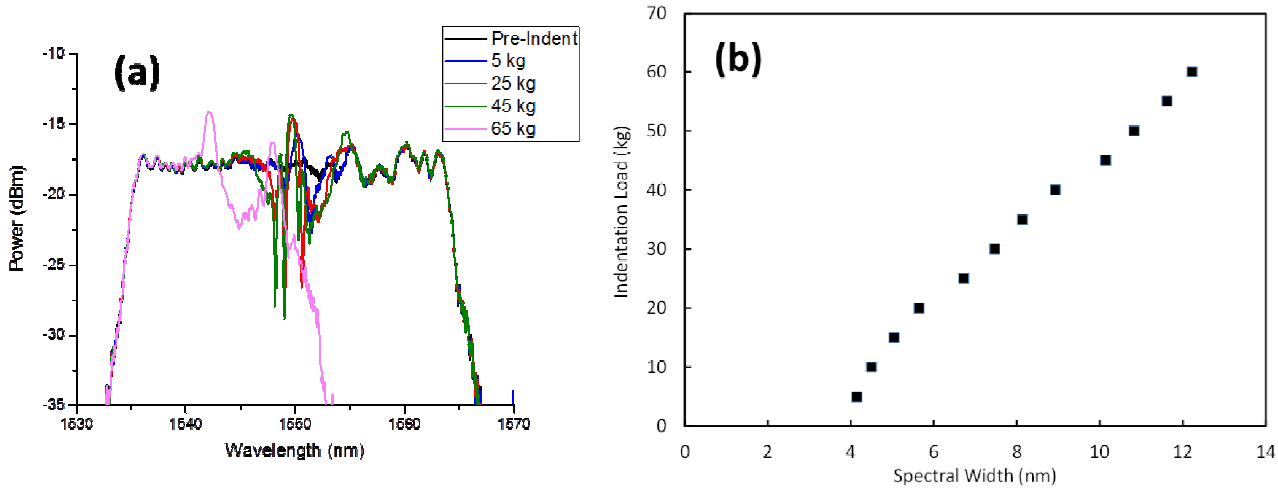

Figure 4. (a) Reflected spectra of centered, chirped FBG embedded in epoxy film on alumina coupon measured post-indentation for various indentation loads. **(b)** Indentation load compared to the spectral width over which the corresponding post-indent spectrum deviates from its pre-indent spectrum.

3.2 Thermally-Induced Delamination

Figure 5 shows the results of a typical test in which an epoxy film with an embedded, chirped FBG on mold-released alumina is cooled to low temperature. The epoxy film in this particular example is approximately 500 μm thick. Prior to the application of the epoxy film, a 0.5 μL drop of Ultra II mold release was placed on the center of the alumina coupon and allowed to dry, leaving a circular mold-released region of diameter ~ 4 mm. The FBG is then positioned such that the grating lies above this mold-released region, as illustrated in Figure 1(b). Upon moderate cooling to −95 °C, the reflected spectrum exhibits a uniform shift of −1.60 nm (measured at the high-wavelength spectral edge), indicating a uniform axial strain profile across the grating. If we assume that the thermal expansion of the entire coupon is dominated by the rigid alumina substrate ($\alpha = 3.6\times10^{-6}$ °C $^{-1}$) and that no delamination occurs, then the expected wavelength shift from this extent of cooling is given by $\Delta\lambda_B = [(1\text{-}P_e)\alpha + \xi] \times\Delta T\times\lambda_B = 1.61$ nm,[39] using a photoelastic constant (P_e) of 0.22[36] and a thermo-optic coefficient (ξ) of 5.81×10^{-6} °C $^{-1}$.[40] The excellent agreement between this calculated value and the observed shift indeed confirms that no delamination occurs with moderate cooling. However, upon severe cooling to −196 °C, the reflected spectrum exhibits characteristics of a non-uniform strain distribution. Visual observation of the coupon clearly reveals that the epoxy film has delaminated from the alumina substrate within the mold-released region. The thermal stress due to the mismatch between the film and substrate coefficients of thermal expansion apparently reaches a critical level during severe cooling, such that the stress is relieved by preferential delamination along this zone of poor adhesion. As with mechanically-induced delamination, thermally-induced delamination is accompanied by the development of a non-uniform strain distribution in the overlying film. Again, the reflected spectrum suggests both compressive and tensile elements to the strain distribution. More specifically, the central portion of the spectrum appears to shift to lower wavelengths, yet the high-wavelength spectral edge has shifted to higher wavelengths (relative to the −95 °C spectrum), indicative of compressive and tensile strain, respectively.

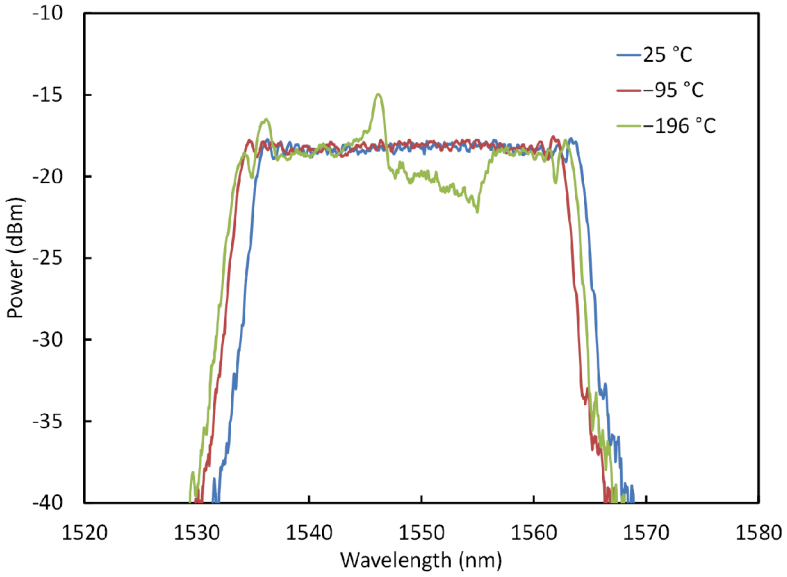

Figure 5. Reflected spectra from a chirped FBG embedded in epoxy film on partially mold-released alumina coupon at 25 °C (blue), cooled to −95 °C in an environmental chamber (red), and cooled to −196 °C by immersion in liquid nitrogen (green). The diameter of the mold-released region is approximately 4 mm, and the grating is embedded over the mold-released interface.

To compare thermally-induced delamination with mechanically-induced delamination, we analyzed reflected spectra taken at room temperature before and after severe cooling in liquid nitrogen (Figure 6). We further varied the size of the delamination by controlling the amount of mold release applied to the starting coupon. As before, this analysis provides information regarding the permanent deformation in the film associated with delamination. Figure 6(a) shows that, in the absence of a region of poor adhesion, no preferential delamination occurs and the reflected spectra before and after cooling are identical, *i.e.*, there is no residual strain in the film. Conversely, the mold-released coupons (Figure 6(b) and Figure 6(c)) preferentially delaminate and the reflected spectra reveal a residual, non-uniform strain distribution. The spectral width over which the spectra deviate before and after cooling clearly scales with the size of the delamination, similar to mechanically-induced delamination. On the other hand, the residual strain is predominantly compressive, in contrast with the residual tensile strain distributions observed during indentation tests.

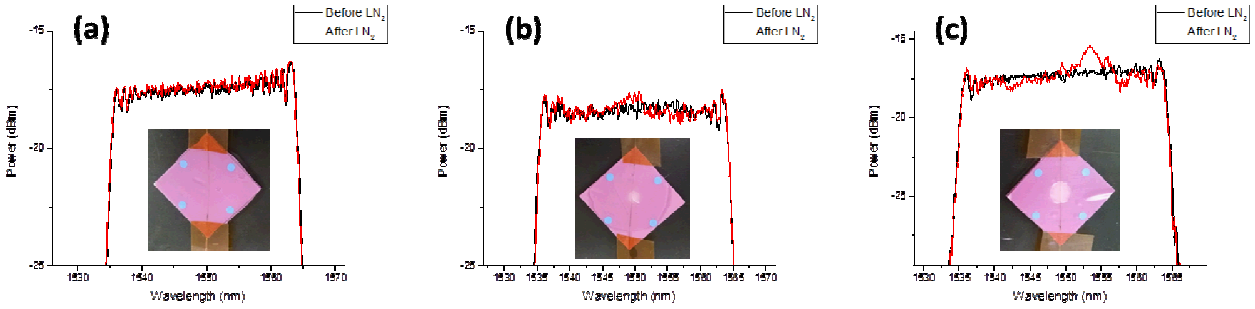

Figure 6. Reflected spectra from chirped FBGs embedded in epoxy films on partially mold-released alumina coupons before (black) and after (red) cooling to −196 °C by immersion in liquid nitrogen. The diameters of the mold-released region are: **(a)** 0 mm (no mold release), **(b)** 4 mm, **(c)** 7 mm. All spectra were recorded at room temperature. Each corresponding image shows a plane-view of the coupon taken after cooling.

In Figure 7, the spectra measured post-cooling from Figure 6(b) and Figure 6(c) are compared to calculated spectra. To maintain consistency with our previous analysis (Figure 3), we applied Gaussian strain distributions to the OptiGrating calculations, varying the width and height of the distributions. The strain distributions plotted in Figure 7(c) provide a reasonable qualitative match to the experimental data, although they are by no means quantitatively accurate. Nevertheless, there again appears to be remarkable consistency between the known delamination size and spectrally-

estimated quantities. For the 4 mm and 7 mm delaminations, the residual strain distributions span approximately 3.4 mm and 6.6 mm, respectively.

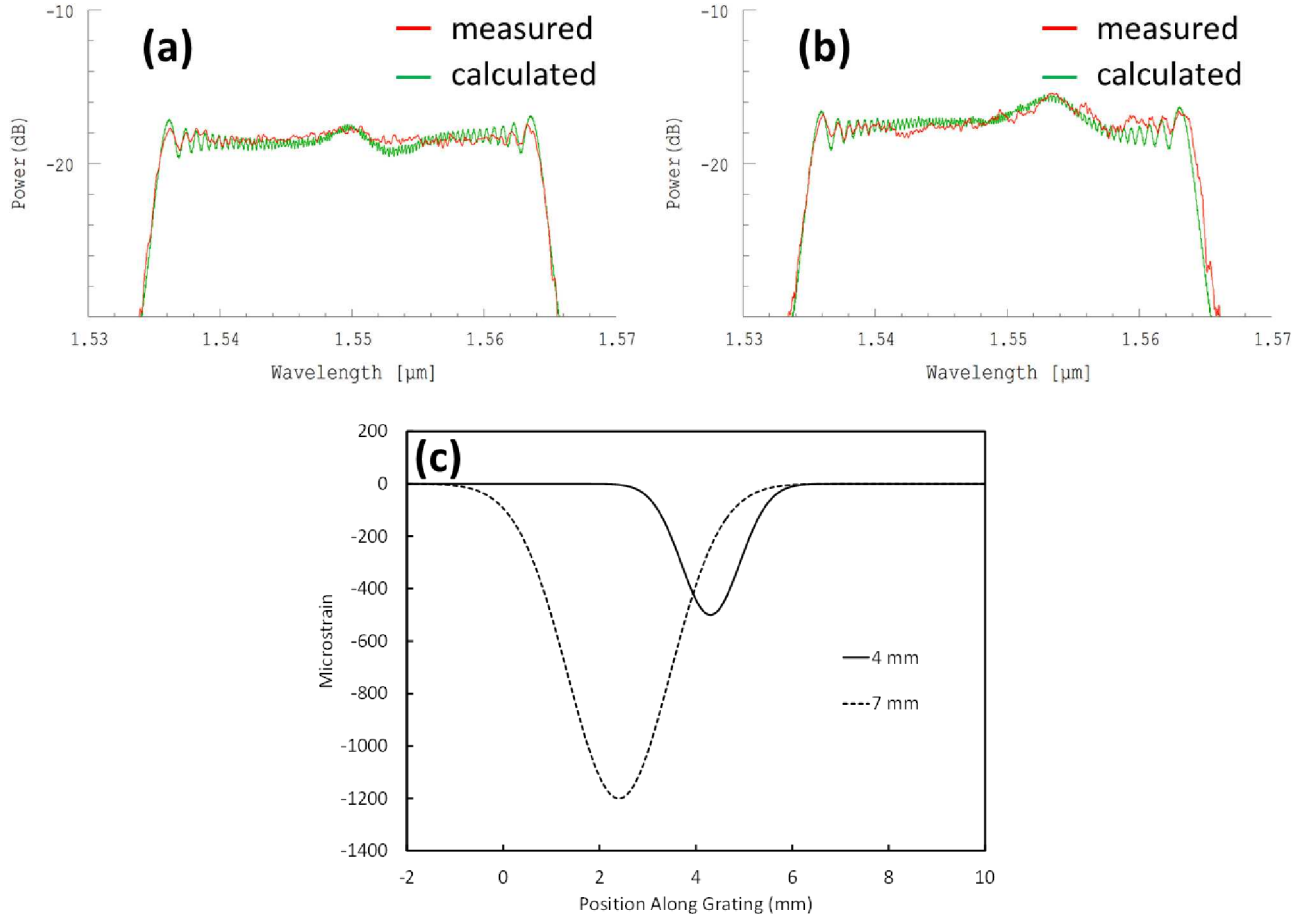

Figure 7. (a),(b) Measured reflected spectra (red) from chirped FBGs embedded in epoxy films on partially mold-released alumina coupons after cooling to −196 °C by immersion in liquid nitrogen, compared to spectra calculated using OptiGrating software (green). The experimental data correspond to the post-cooling curves for **(a)** 4 mm and **(b)** 7 mm delaminations plotted in Figure 6(b) and Figure 6(c), respectively. The axial strain profiles used for the calculations are plotted in **(c)**.

Finally, we attempted to study the effect of film thickness on thermally-induced delaminations and the accompanying spectral response from embedded FBGs. Figure 8 shows a series of partially mold-released coupons of increasing film thickness after severe cooling. At the lowest film thickness, 413 μm, cooling induces delamination, but only within a portion of the mold-released region. At the second lowest film thickness, 464 μm, the delaminated area increases, but it is still restricted within the mold-released region. At the larger film thicknesses, the mold-released region completely delaminates, but extensive delamination is also observed across the entirety of the film, as well as significant cohesive failure (cracking) through the film thickness. This is, in fact, an expected result, as the strain energy release rate resulting from cohesive and adhesive film cracking is proportional to the film thickness.[41] Thus, the propensity for cracking increases with increasing film thickness. In the context of these experiments, for a constant cooling magnitude, additional stress relief mechanisms are activated in thicker films. Unfortunately, however, the cohesive failure of thicker films causes fracture of the embedded FBGs, hence we are unable to analyze their spectral response after cooling. We subjected samples with similar film thicknesses to rapid cooling as low as −131 °C in liquid nitrogen/solvent mixtures, as well as slow, controlled cooling to −95 °C in an environmental chamber, but these tests produced no delamination whatsoever. Future experiments will rely on precise control of sample temperature over the range −131 °C to −196 °C to circumvent catastrophic failure mechanisms in these thicker films.

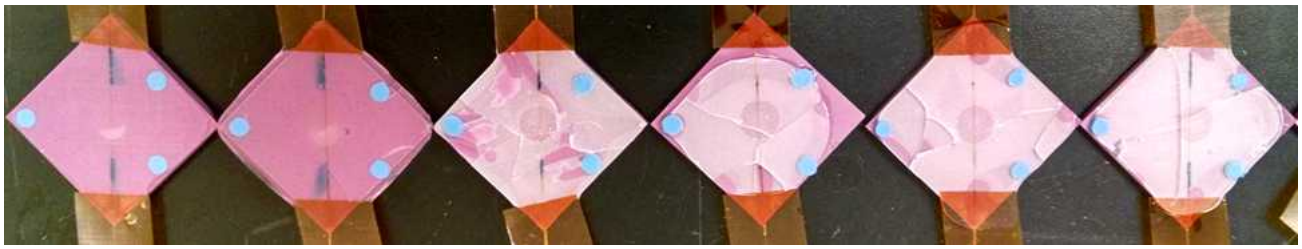

Figure 8. Plane-view images of chirped FBGs embedded in epoxy films of varying thickness on partially mold-released alumina coupons after cooling to −196 °C by immersion in liquid nitrogen. The size of the mold-released region is identical for all coupons. The thicknesses of the epoxy films are, from left to right: 413 μm, 464 μm, 790 μm, 947 μm, 998 μm, and 1320 μm.

4. CONCLUSIONS

In summary, we have exploited the powerful strain-sensing capabilities of embedded FBGs to study delamination at simple, planar interfaces between epoxy films and alumina substrates. We have examined circular delamination induced by two distinct processes, one based on indentation stress and one based on thermal mismatch stress. From a sensing and detection standpoint, we have shown that these delaminations are plainly apparent in chirped FBG reflected spectra, even after the stressing condition is removed, due to a residual, non-uniform strain distribution in the film. The residual strain states inferred from the reflected spectra differ substantially between the two delamination processes and, more broadly, are distinct from other delamination processes studied previously. However, in both cases, we have observed strong correlation between spectrally-derived measurements, such as spectral widths, and delamination size. This outcome adds to the growing body of evidence suggesting that embedded FBGs may be used for universal measurement of delamination size, independent of the physical process by which the delamination is generated.

More generally, our results provide further confirmation that FBGs are an exceptional tool for the detection of local, interfacial phenomena in encapsulant systems. In many such systems, there are extremely limited means available for interrogation of critical interfaces, as the opacity of filled encapsulants or a particular system design precludes visual observation or other forms of non-destructive evaluation. Therefore, FBGs are uniquely positioned to become the state-of-the-art for embedded health monitoring of encapsulant systems. However, as far as delamination is concerned, additional work is necessary to further develop our understanding of the critical factors affecting FBG response, including the orientation and proximity of the FBG relative to the delamination, the dimensions of the encapsulant and its encapsulated components, and the complexity of the interfacial shape and composition.

ACKNOWLEDGEMENTS

We gratefully acknowledge Clay Newton and Thomas Buchheit for use of indentation instrumentation. We also gratefully acknowledge Thomas Buchheit, David Reedy, Patricia Sawyer, Mark Stavig, and Eric Udd for their assistance and helpful discussions. Sandia National Laboratories is a multi-program laboratory managed and operated by Sandia Corporation, a wholly owned subsidiary of Lockheed Martin Corporation, for the U.S. Department of Energy's National Nuclear Security Administration under contract DE-AC04-94AL85000.

REFERENCES

[1] LeBlanc, M., Huang, S. Y., Ohn, M., Measures, R. M., Guemes, A. and Othonos, A., "Distributed strain measurement based on a fiber Bragg grating and its reflection spectrum analysis," Opt. Lett. 21(17), 1405-1407 (1996).

[2] Huang, S., Ohn, M. M., LeBlanc, M. and Measures, R. M., "Continuous arbitrary strain profile measurements with fiber Bragg gratings," Smart Mater. Struct. 7, 248-256 (1998).

[3] Cheng, H.-C. and Lo, Y. L., "Arbitrary strain distribution measurement using a genetic algorithm approach and two fiber Bragg grating intensity spectra," Opt. Commun. 239, 323-332 (2004).
[4] Giaccari, P., Dunkel, G. R., Humbert, L., Botsis, J., Limberger, H. G. and Salathé, R. P., "On a direct determination of non-uniform internal strain fields using fibre Bragg gratings," Smart Mater. Struct. 14, 127-136 (2005).
[5] Cheng, H.-C. and Lo, Y. L., "The synthesis of multiple parameters of arbitrary FBGs via a genetic algorithm and two thermally modulated intensity spectra," J. Lightwave Technol. 23(6), 2158-2168 (2005).
[6] Nand, A., Kitcher, D. J., Wade, S. A., Nguyen, T. B., Baxter, G. W., Jones, R. and Collins, S. F., "Determination of the position of a localized heat source within a chirped fibre Bragg grating using a Fourier transform technique," Meas. Sci. Technol. 17, 1436-1445 (2006).
[7] Kitcher, D. J., Nand, A., Wade, S. A., Jones, R., Baxter, G. W. and Collins, S. F., "Implementation of integration of differences method for extraction of temperature profiles along chirped fibre Bragg gratings," ACOFT/AOS Proc. 57-59 (2006).
[8] Nand, A., Kitcher, D. J., Wade, S. A., Jones, R., Baxter, G. W. and Collins, S. F., "Localized strain measurements using an integration method to process intensity reflection spectra from a chirped FBG," Proc. SPIE 6619, 661911 (2007).
[9] Zhang, R., Zheng, S. and Xia, Y., "Strain profile reconstruction of fiber Bragg grating with gradient using chaos genetic algorithm and modified transfer matrix formulation," Opt. Commun. 281, 3476-3485 (2008).
[10] Rodriguez-Cobo, L., Cobo, A. and Lopez-Higuera, J. M., "Recovering a fiber Bragg grating axial strain distribution from its reflection spectrum," Opt. Lett. 38(13), 2327-2329 (2013).
[11] Zheng, S., Zhang, N., Xia, Y. and Wang, H., "Research on non-uniform strain profile reconstruction along fiber Bragg grating via genetic programming algorithm and interrelated experimental verification," Opt. Commun. 315, 338-346 (2014).
[12] Hill, K. O., Malo, B., Bilodeau, F., Johnson, D. C. and Albert, J., "Bragg gratings fabricated in monomode photosensitive optical fiber by UV exposure through a phase mask," Appl. Phys. Lett. 62, 1035-1037 (1993).
[13] Morey, W. W., Meltz, G. and Glenn, W. H., "Fiber optic Bragg grating sensors," Proc. SPIE 1169, 98-107 (1989).
[14] Othonos, A., "Fiber Bragg gratings," Rev. Sci. Instrum. 68, 4309-4341 (1997).
[15] Black, R. J., Zare, D., Oblea, L., Park, Y.-L., Moslehi, B. and Neslen, C., "On the gage factor for optical fiber grating strain gages," SAMPE'08, 18-122 (2008).
[16] Leduc, D., Lecieux, Y., Morvan, P.-A. and Lupi, C., "Architecture of optical fiber sensor for the simultaneous measurement of axial and radial strain," Smart. Mater. Struct. 22, 075002 (2013).
[17] Okabe, Y., Yashiro, S., Kosaka, T. and Takeda, N., "Detection of transverse cracks in CFRP composites using embedded fiber Bragg grating sensors," Smart Mater. Struct. 9, 832-838 (2000).
[18] Satori, K., Ikeda, Y., Kurosawa, Y., Hongo, A. and Takeda, N., "Development of small-diameter optical fiber sensors for damage detection in composite laminates," Proc. SPIE 3986, 104-111 (2000).
[19] Takeda, S., Okabe, Y. and Takeda, N., "Delamination detection in CFRP laminates with embedded small-diameter fiber Bragg grating sensors," Compos. A 33, 971-980 (2002).
[20] Okabe, Y., Mizutani, T., Yashiro, S. and Takeda, N., "Detection of microscopic damages in composite laminates with embedded small-diameter fiber Bragg grating sensors," Compos. Sci. Technol. 62, 951-958 (2002).
[21] Leng, J. S. and Asundi, A., "Real-time cure monitoring of smart composite materials using extrinsic Fabry-Perot interferometer and fiber Bragg grating sensors," Smart Mater. Struct. 11, 249-255 (2002).
[22] Takeda, S., Okabe, Y. and Takeda, N., "Application of chirped FBG sensors for detection of local delamination in composite laminates," Proc. SPIE 5050, 171-178 (2003).
[23] Takeda, S., Okabe, Y., Yamamoto, T. and Takeda, N., "Detection of edge delamination in CFRP laminates under cyclic loading using small-diameter FBG sensors," Compos. Sci. Technol. 63, 1885-1894 (2003).
[24] Mizutani, T., Okabe, Y. and Takeda, N., "Quantitative evaluation of transverse cracks in carbon fiber reinforced plastic quasi-isotropic laminates with embedded small-diameter fiber Bragg grating sensors," Smart Mater. Struct. 12, 898-903 (2003).
[25] Okabe, Y., Tsuji, R. and Takeda, N., "Application of chirped fiber Bragg grating sensors for identification of crack locations in composites," Compos. A 35, 59-65 (2004).
[26] Yashiro, S., Takeda, N., Okabe, T. and Sekine, H., "A new approach to predicting multiple damage states in composite laminates with embedded FBG sensors," Compos. Sci. Technol. 65, 659-667 (2005).
[27] Takeda, S., Minakuchi, S., Okabe, Y. and Takeda, N., "Delamination monitoring of laminated composites subjected to low-velocity impact using small-diameter FBG sensors," Compos. A 36, 903-908 (2005).

[28] Takeda, N., Okabe, Y., Kuwahara, J., Kojima, S. and Ogisu, T., "Development of smart composite structures with small-diameter fiber Bragg grating sensors for damage detection: Quantitative evaluation of delamination length in CFRP laminates using Lamb wave sensing," Compos. Sci. Technol. 65, 2575-2587 (2005).
[29] Takeda, N., Yashiro, S. and Okabe, T., "Estimation of the damage patterns in notched laminates with embedded FBG sensors," Compos. Sci. Technol. 66, 684-693 (2006).
[30] Yashiro, S., Okabe, T. and Takeda, N., "Damage identification in a holed CFRP laminate using a chirped fiber Bragg grating sensor," Compos. Sci. Technol. 67, 286-295 (2007).
[31] Sanderson, A. R., Ogin, S. L., Crocombe, A. D., Gower, M. R. L. and Lee, R. J., "Use of a surface-mounted chirped fibre Bragg grating sensor to monitor delamination growth in a double-cantilever beam test," Compos. Sci. Technol. 72, 1121-1126 (2012).
[32] Riccio, A., Raimondo, A., Fragale, S., Camerlingo, F., Gambino, B., Toscano, C. and Tescione, D., "Delamination buckling and growth phenomena in stiffened composite panels under compression. Part I: An experimental study," J. Compos. Mater. 48(23), 2843-2855 (2014).
[33] Antonucci, V., Esposito, M., Ricciardi, M. R., Giordano, M. and Zarrelli, M., "Strain monitoring of composite elements by fibre Bragg grating sensors during a quasi-static indentation," Compos. B 56, 34-41 (2014).
[34] Huang, W. P., "Coupled-mode theory for optical waveguides: An overview," J. Opt. Soc. Am. A 11(3), 963-983 (1994).
[35] Marshall, D. B. and Evans, A. G., "Measurement of adherence of residually stress thin films by indentation. I. Mechanics of interface delamination," J. Appl. Phys. 56, 2632-2638 (1984).
[36] Yu-Lung, L. and Han-Sheng, C., "Measurement of thermal expansion coefficients using an in-fibre Bragg-grating sensor," Meas. Sci. Technol. 9, 1543-1547 (1998).
[37] Kim, K. T., Kim, I. S., Lee, C.-H. and Lee, J., "A temperature-insensitive cladding-etched fiber Bragg grating using a liquid mixture with a negative thermo-optic coefficient," Sensors 12(6), 7886-7892 (2012).
[38] Hutchins, K. I., "Measurement of interfacial adhesion in glass-epoxy systems using the indentation method," M.S. Thesis, University of New Mexico (2015).
[39] Yeo, T. L., Sun, T., Grattan, K. T. V., Parry, D., Lade, R. and Powell, B. D., "Characterisation of a polymer-coated fiber Bragg grating sensor for relative humidity sensing," Sens. Actuat. B 110, 148-155 (2005).
[40] Kronenberg, P., Rastogi, P. K., Giaccari, P. and Limberger, H. G., "Relative humidity sensor with optical fiber Bragg gratings," Opt. Lett. 27(16), 1385-1387 (2002).
[41] Hutchinson, J. W. and Suo, Z., "Mixed Mode Cracking in Layered Materials," Adv. Appl. Mech. 29, 63-191 (1992).